# Functional interactions of voltage sensor charges with an S2 hydrophobic plug in hERG channels

Yen May Cheng, Christina M. Hull, Christine M. Niven, Ji Qi, Charlene R. Allard, and Tom W. Claydon

Department of Biomedical Physiology and Kinesiology, Simon Fraser University, Burnaby, British Columbia V5A 1S6, Canada

Human ether-à-go-go–related gene (hERG, Kv11.1) potassium channels have unusually slow activation and deactivation kinetics. It has been suggested that, in fast-activating *Shaker* channels, a highly conserved Phe residue (F290) in the S2 segment forms a putative gating charge transfer center that interacts with S4 gating charges, i.e., R362 (R1) and K374 (K5), and catalyzes their movement across the focused electric field. F290 is conserved in hERG (F463), but the relevant residues in the hERG S4 are reversed, i.e., K525 (K1) and R537 (R5), and there is an extra positive charge adjacent to R537 (i.e., K538). We have examined whether hERG channels possess a transfer center similar to that described in *Shaker* and if these S4 charge differences contribute to slow gating in hERG channels. Of five hERG F463 hydrophobic substitutions tested, F463W and F463Y shifted the conductance–voltage (G-V) relationship to more depolarized potentials and dramatically slowed channel activation. With the S4 residue reversals (i.e., K525, R537) taken into account, the closed state stabilization by F463W is consistent with a role for F463 that is similar to that described for F290 in *Shaker*. As predicted from results with *Shaker*, the hERG K525R mutation destabilized the closed state. However, hERG R537K did not stabilize the open state as predicted. Instead, we found the neighboring K538 residue to be critical for open state stabilization, as K538R dramatically slowed and right-shifted the voltage dependence of activation. Finally, double mutant cycle analysis on the G-V curves of F463W/K525R and F463W/K538R double mutations suggests that F463 forms functional interactions with K525 and K538 in the S4 segment. Collectively, these data suggest a role for F463 in mediating closed–open equilibria, similar to that proposed for F290 in *Shaker* channels.

The Journal of General Physiology

## INTRODUCTION

Kv11.1 or human ether-à-go-go–related gene (hERG) potassium channels underlie the cardiac delayed rectifier current, $I_{Kr}$, which is critical for membrane repolarization and termination of the ventricular action potential (Sanguinetti and Jurkiewicz, 1990; Sanguinetti et al., 1995; Trudeau et al., 1995). The unusual gating properties of hERG channels make them uniquely suited to their function in cardiac repolarization. During depolarization, slow activation with concomitant rapid inactivation results in limited outward current; upon repolarization, rapid recovery from inactivation and slow deactivation results in large tail currents that contribute to further membrane repolarization (Sanguinetti and Jurkiewicz, 1990). The importance of understanding hERG channel function is highlighted by the link between loss-of-function mutations or drug block of hERG channels with congenital or acquired long QT syndrome, an arrhythmia linked to sudden cardiac death (Curran et al., 1995; Sanguinetti et al., 1995; for review see Sanguinetti and Tristani-Firouzi, 2006). However, compared with the archetypal *Shaker* channel and other closely related members of the Kv1 family that activate and deactivate relatively quickly, the mechanisms regulating hERG channel gating are poorly understood.

Like other voltage-gated potassium (Kv) channels, *Shaker* and hERG are composed of a tetrameric assembly of identical α subunits around a central ion-conducting pore (Jiang et al., 2003; Long et al., 2005, 2007; Chen et al., 2010). Each α subunit has six transmembrane helical segments, S1–S6, and cytoplasmic N- and C-terminal domains. The ability to detect changes in voltage is conferred by the voltage-sensing domain (VSD) formed by segments S1–S4, whereas ion conduction is achieved through the pore domain formed by S5–S6. Within the VSD, the S4 segment has the important distinction of containing four to eight regularly spaced basic residues (Arg or Lys). In response to changes in the membrane potential, these gating charges traverse a focused electric field (Liman et al., 1991; Papazian et al., 1991; Starace and Bezanilla, 2004; Ahern and Horn, 2005) and drive conformational changes in the VSD as well as in the pore domain to open or close the channel (Lu et al., 2002; Long et al., 2005; Chen et al., 2010). The S1–S3 helices of the VSD contain several negatively charged residues that are thought to shape the transmembrane electric field and contribute to stabilizing the S4 charges within

Correspondence to Thomas W. Claydon: thomas_claydon@sfu.ca
Abbreviation used in this paper: VSD, voltage-sensing domain.



The Rockefeller University Press $30.00
J. Gen. Physiol. Vol. 142 No. 3 289–303
www.jgp.org/cgi/doi/10.1085/jgp.201310992

the hydrophobic environment of the lipid membrane (Tiwari-Woodruff et al., 1997; Long et al., 2005; Zhang et al., 2005; Piper et al., 2008; Pless et al., 2011).

The role of a highly conserved Phe residue in S2 (F290 in *Shaker*) that forms part of the hydrophobic barrier within the VSD and about which the electric field is thought to be focused has received considerable recent interest (Long et al., 2005; Chen et al., 2010; Tao et al., 2010). It has been suggested that a gating charge transfer center formed in large part by F290 in *Shaker* channels catalyzes the sequential movement of S4 gating charges across the electric field (Tao et al., 2010), although the precise nature of the interaction remains unclear. An electrostatic cation–π interaction between the native Phe residue and S4 charges has been shown to be unlikely (Tao et al., 2010; Lacroix and Bezanilla, 2011; Pless et al., 2011). It has been shown, however, that substituting a Trp residue for position 290 leads to a dramatic stabilization of the open state, likely by inducing a cation–π interaction between the substituted Trp and the Lys residue (K374; K5) at the base of the S4 segment (Tao et al., 2010; Pless et al., 2011). More recently, the question of whether F290 regulates the transfer of each S4 gating charge (i.e., R1–R4) in WT *Shaker* or only a more limited transfer of the late charge component carried by R4 (Lacroix and Bezanilla, 2011) has been discussed.

To date, there is little information regarding the importance of a gating charge transfer center in Kv channels outside the Kv1 family. However, the pertinent Phe residue in S2 is well conserved across Kv channel families, raising the question of how this residue might catalyze gating charge transfer in other channels, particularly those with voltage-dependent gating characteristics that are distinct from those of the Kv1 family. In hERG channels, for example, the S2 Phe residue is conserved (F463; Fig. 1); however, hERG channels activate and deactivate very slowly compared with *Shaker* channels. This suggests that differences in the charges moving through the transfer center may contribute to the unusually slow gating. Transposing the outer and inner S4 charges, i.e., R362K/K374R (R1K/K5R), in the background of the F290W mutation in *Shaker* resulted in a dramatic slowing of channel activation, accelerated deactivation, and right-shifted gating charge movement (Tao et al., 2010). These results suggest that the presence of a Lys residue at the outer, but not the inner, S4 segment results in a relative stabilization of the resting state of the voltage sensor, and thus the closed state of the channel. Interestingly, hERG channels have a Lys residue at both the outer (K525) and inner (K538) boundaries of the S4 segment, although the Arg residue immediately adjacent to K538 (R537) aligns better with the repeating sequence of S4 gating charges (i.e., KxxRxxRxxRxxR$^{537}$K$^{538}$) and, thus, with *Shaker* K5 (Fig. 1). Based on these observations, we have first examined whether voltage-dependent gating of hERG channels is regulated by the S2 Phe residue, F463, in a manner similar to that of the proposed gating charge transfer center in *Shaker* channels. Second, we have assessed the possibility that the distinct gating behaviors of hERG and *Shaker* channels are due in part to the different positively charged residues at the outer and inner margins of the S4 segments. We show that substitution of F463 with bulky, cyclic hydrophobic residues shifts the voltage dependence of hERG activation in a way that is consistent with that predicted from results observed in *Shaker* channels. Moreover, we found that charge conserving mutations of K525 and K538 affected the relative stabilities of the closed and open states, which is consistent with a key role for Lys residues at the margins of S4 in voltage sensor resting and activated configurations. Finally, we provide evidence in support of functional interactions between F463 and K525 or K538, which is indicative of a role for the S2 Phe residue in the modulation of voltage-dependent S4 movement in hERG channels.

## MATERIALS AND METHODS

### Molecular biology

WT and mutant hERG1a channels were expressed in *Xenopus laevis* oocytes using a pBluescript SKII expression vector. Mutant hERG constructs were generated using conventional overlap extension PCR. All mutagenic primers were synthesized by Sigma-Aldrich, and constructs were sequenced by Eurofins MWG Operon. hERG construct cDNA was linearized with XbaI restriction endonucleases (Thermo Fisher Scientific) and used with the mMessage mMachine T7 Ultra transcription kit (Ambion) to synthesize cRNA.


**Figure 1.** Highly conserved amino acids in the S2 and S4 segments. Sequence alignment of the S2 region (left) and the S4 voltage sensor (right) of *Shaker* and hERG channels. Conserved residues forming the putative gating charge transfer center in S2 are highlighted in green. The positive S4 residues investigated in this study are highlighted in blue. The remaining S4 charges are shown in bold font. The conserved negative residues in S2 suggested to contribute to the gating charge transfer center in *Shaker* channels (i.e., E293) are shown in red.

### Oocyte preparation and expression

In accordance with the policies and procedures of the Simon Fraser University Animal Care Committee and the Canadian Council of Animal Care, *X. laevis* frogs were terminally anaesthetized by immersion in 1 liter of 2 g/liter tricaine methanesulphonate solution (with 5 mM HEPES; titrated to pH 7.4) for 25 min, and their oocytes were removed. Stage V–VI oocytes were isolated using a combination of collagenase treatment (~1 h in 1 mg/ml collagenase type 1A in $MgOR_2$ solution [in mM: 96 NaCl, 2 KCl, 20 $MgCl_2$, and 5 HEPES, titrated to pH 7.4 with NaOH]) and manual defolliculation. Defolliculated oocytes were injected with 50 nl cRNA (at concentrations of 0.1–2 µg/µl) using a Drummond digital microdispenser (Drummond Scientific) and incubated in SOS+ media (in mM: 96 NaCl, 2 KCl, 1.8 $CaCl_2$, 1 $MgCl_2$, 5 HEPES, 5% horse serum, 2.5 sodium pyruvate, and 100 mg/ml gentamicin sulfate, titrated to pH 7.4 with NaOH) at 19°C for 1–4 d before recordings. All chemicals were purchased from Sigma-Aldrich.

### Electrophysiology and data analysis

Whole-cell membrane current recordings from oocytes expressing hERG constructs were performed using conventional two-electrode voltage clamp with an Axoclamp 900A amplifier, Digidata 1440 interface, and pClamp 10 software (Axon Instruments; Molecular Devices). Microelectrodes were made with thin-walled borosilicate glass (World Precision Instruments) and had resistances of 0.2 – 2.0 MΩ when filled with 3 M KCl. Current signals were low-pass filtered at 4 kHz (−3 dB, 8 pole Bessel filter) and digitized (16-bit) at a 10-kHz sampling frequency. Depending on the mutant being studied, cells were held at −130 mV or −80 mV. Voltage protocols are described in the relevant text and figure legends. Current recordings were performed at room temperature (20−22°C), during which oocytes were bathed in ND96 solution (in mM: 96 NaCl, 3 KCl, 1 $MgCl_2$, 0.5 $CaCl_2$, and 5 HEPES, titrated to pH 7.4 with NaOH). All reagents were purchased from Sigma-Aldrich. Unless noted otherwise, capacity transients were deleted for clarity and current traces are shown without leak subtraction.

Conductance–voltage (G-V) relationships for hERG channels were derived using standard tail current analysis. Cells were depolarized to potentials in the range of −130 mV to +60 mV and tail currents measured at −60 mV, or at −110 mV if there was appreciable channel opening at −60 mV. Depolarizing pulses of 2 s were usually adequate to activate most constructs. However, for mutants with slow activation kinetics, the duration of the depolarizing steps was increased to 10 or 15 s to avoid an artificial depolarizing shift in the voltage dependence of activation caused by incomplete channel activation. Tail current amplitudes at each potential were normalized to the maximum tail current value for an estimate of the normalized conductance. Parameters for voltage-dependent activation were derived from fits of G-V relationships to the Boltzmann function:

$$y = 1 / \left\{1 + \exp\left[\left(V_{1/2} - V\right) / k\right]\right\}, \quad (1)$$

where $y$ is the normalized conductance, $V$ is the test potential, $V_{1/2}$ is the half-activation potential, and $k$ is the slope factor. $k$ is equal to RT/$z$F, where $z$ is the apparent number of gating charges, R is the universal gas constant, F is Faraday's constant, and T is absolute temperature. Reported $V_{1/2}$ and $k$ values represent means ± SEM derived from the Boltzmann fits to data from multiple cells.

$V_{1/2}$ and $z$ values for each construct were used to estimate the free energy difference at 0 mV ($\Delta G_0$) between the closed and open states of the activation gate as follows (Li-Smerin et al., 2000):

$$\Delta G_0 = zFV_{1/2}. \quad (2)$$

$\Delta G_0$ may also be referred to as the chemical potential difference between the open and closed states in the absence of an electric field. This approach is somewhat limited by the fact that $z$ values calculated from Boltzmann fits of steady-state ionic data typically underestimate the actual amount of gating charge moved during activation and the oversimplifying assumption inherent in the use of the Boltzmann function that channel activation is a simple two-state process. Although it has recently been shown that measurement of the median voltage of charge transfer ($V_m$) from gating current recordings may provide a more accurate estimate of the net free energy difference involved in channel opening without the limitations associated with Boltzmann fits (Chowdhury and Chanda, 2012), Eq. 2 provides the best available method to derive $\Delta G_0$ values from our steady-state ionic current data. To account for shifts in the voltage dependence of steady-state activation and $\Delta G_0$, the rates of current activation and deactivation were plotted against the total electrochemical potential energy for activation at each test voltage, i.e., $-(\Delta G_0 - zFV)$, rather than the test voltage directly. Finally, the change in the free energy difference at 0 mV ($\Delta\Delta G_0$) caused by a mutation can be calculated as:

$$\Delta\Delta G = \Delta G_0^{\,mut} - \Delta G_0^{\,WT}, \quad (3)$$

$$\text{SE of } \Delta\Delta G_0 = \sqrt{\left[\left(\text{SE of } \Delta G_0^{\,mut}\right)^2 + \left(\text{SE of } \Delta G_0^{\,WT}\right)^2\right]}, \quad (4)$$

where $\Delta G_0^{mut}$ and $\Delta G_0^{WT}$ are the chemical potentials for activation of the mutant and WT channels, respectively, and SE is the standard error (Li-Smerin et al., 2000; Piper et al., 2005).

Double mutant cycle analysis was used to determine whether the effects of two mutations (mut1 and mut2) were additive and, thus, whether a functional interaction existed between the two mutation sites. To this end, the degree of nonadditivity ($\Delta\Delta G_{0,NA}$) was calculated as:

$$\Delta\Delta G_{0,NA} = \left|\Delta G_0^{\,mut1} + \Delta G_0^{\,mut2} - \Delta G_0^{\,WT} - \Delta G_0^{\,mut1,2}\right|. \quad (5)$$

The SE value for $\Delta\Delta G_{0,NA}$ was calculated as the square root of the sum of the squares of the SE values for each of the four $\Delta G_0$. Nonadditivity was defined as a $\Delta\Delta G_{0,NA} > 4.2$ kJ mol$^{-1}$ (Zhang et al., 2005).

To quantify deactivation kinetics, the decaying portion of tail currents (see Fig. 3 B) was fitted to a biexponential function of the form: $I = A_1 e^{-t/\tau 1} + A_2 e^{-t/\tau 2} + C$, where $I$ is the current amplitude, $t$ is time, $A_1$ and $A_2$ and $\tau_1$ and $\tau_2$ are the amplitudes and time constants for the slow and fast components, respectively, and $C$ is a constant. For ease of comparison across multiple mutants, the weighted mean of the time constants was then calculated as: $\tau_{deact} = (A_1\tau_1 + A_2\tau_2)/(A_1 + A_2)$.

Curve fitting and statistical comparisons were performed in pClamp 10 or SigmaPlot 11.0 (Systat Software, Inc.). Unless otherwise noted, data are shown as the mean ± SEM. $n$ represents the number of oocytes tested.

## RESULTS

### Effects of hydrophobic substitutions of the conserved F463 residue in S2

To assess whether the hERG F463 residue regulates S4 movement, as suggested for the homologous F290 residue in *Shaker* channels, we characterized the effects of five hydrophobic F463 mutants (F to M, W, L, Y, and V) on hERG gating. These residues were chosen based on the reported dependence of S4 movement in *Shaker* on

the hydrophobicity of the residue at position 290 (Lacroix and Bezanilla, 2011). Fig. 2 A displays typical current families recorded from oocytes expressing WT and two mutant channels in response to typical activation protocols. Tail currents from experiments like those in Fig. 2 A were normalized to the maximal tail current amplitude to derive the G-V curves shown in Fig. 2 B. Compared with WT, F463M activated at slightly more negative potentials and had a faster rate of deactivation at −60 mV. However, these effects were small compared with the dramatic decrease in the activation rate of F463W channels, which necessitated increasing the duration of the activating voltage step from 2 to 15 s. In response to 2-s depolarizing voltage steps, the F463M, -L, and -V mutants exhibited relatively small changes in the voltage dependence of activation when compared with WT hERG. In contrast, the G-V curves for F463W and -Y channels, which were obtained using 15-s voltage steps, were quite right-shifted; F463W also exhibited a decrease in the slope of the relationship. Mean values of $V_{1/2}$ and $k$ from fits of the G-V curves to a Boltzmann function are summarized in Table 1. We also calculated the $\Delta\Delta G_0$ for each mutant, which takes into account the shift in both $V_{1/2}$ and $k$ (Table 1), to quantify the total perturbation of steady-state activation. To do this, we paired mutant data with WT data recorded using a similar pulse duration because, consistent with previous studies (Schönherr et al., 1999; Viloria et al., 2000), increasing the pulse duration from 2 to 10 or 15 s caused a small left-shift of the $V_{1/2}$ and a slight decrease in the $k$ value for the G-V relationship of WT hERG channels, and resulted in slightly different $\Delta G_0$ values (Fig. 2 B and Table 1). Of the five mutants, only F463W and F463Y resulted in a significant shift in the relative stabilities of the open and closed states of the channel, which we defined as a $|\Delta\Delta G_0| > 4.2$ kJ mol$^{-1}$ ($\sim$1 kcal mol$^{-1}$). The large, positive $\Delta\Delta G_0$ values for F463W and F463Y suggest an increase in the relative stability of the closed state compared with the open state. Conversely, a large negative $\Delta\Delta G_0$ implies a stabilization of the open state relative to the closed state.

The effects of the F463 mutants on activation and deactivation time courses are presented in Fig. 3. Due to the concomitant activation and inactivation of hERG channels during depolarizing steps, activation kinetics were measured using an envelope of tails protocol (Fig. 3 A), and the time constant for activation ($\tau_{act}$) at each test potential was obtained from fits of the peak tail currents to a single exponential function. Deactivation time courses ($\tau_{deact}$) were obtained using a standard two-pulse protocol (Fig. 3 B); the reported $\tau_{deact}$ value represents a weighted mean of the fast and slow time constants derived from biexponential fits to the tail currents (see Materials and methods). To account for shifts in the voltage dependence of steady-state activation, $\tau_{act}$ and $\tau_{deact}$ values were plotted against the calculated electrochemical potential energy for activation at each test voltage. As with steady-state activation, F463M, -V, and -L had only minor effects on $\tau_{act}$ values over the voltage range studied, whereas F463W

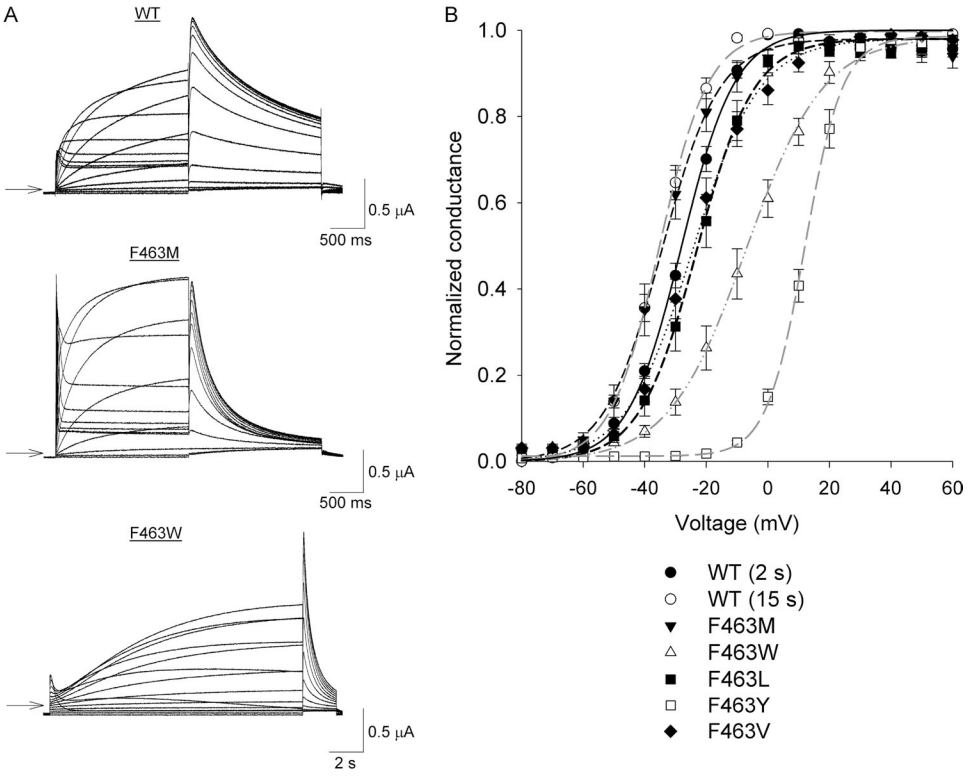


**Figure 2.** Bulky, aromatic substitutions of hERG F463 alter voltage-dependent gating. (A) Typical current traces recorded from WT and mutant hERG channels. Oocytes were held at −80 mV and subjected to either 2- or 15-s depolarizing steps to +60 V in 10-mV increments. Tail currents were recorded during a 2-s pulse to −60 mV. Arrows indicate the zero current level. Note the change in scale for F463W. (B) Effects of the F463 mutations on the G-V relationship. Peak tail currents from experiments such as those in A were normalized to the maximum peak tail current to provide a measure of conductance. WT data recorded using both 2- and 15-s pulses are shown to allow for comparisons with mutant G-V curves obtained using different pulse durations. Data points represent means ± SEM (error bars). Solid and broken lines indicate fits of the data to a Boltzmann function (see Materials and methods). $n$ values and parameters from the Boltzmann fits are summarized in Table 1.

and -Y dramatically altered $\tau_{act}$, increasing the value 10–25× at any given electrochemical potential (Fig. 3 C). In contrast to their effects on activation, the F463W and -Y mutations had only small effects on $\tau_{deact}$, whereas the F463M, -V, and -L mutants caused an ∼10× decrease in the value of $\tau_{deact}$ at any given electrochemical potential (Fig. 3 D).

Overall, the large right-shift of the G-V relationships and dramatic slowing of activation by the F463W and -Y mutations suggest that substitution of bulky, aromatic residues at position 463 stabilize the closed state of the channel. The impeded activation of hERG F463W channels appears at first glance to be inconsistent with the behavior of the analogous *Shaker* F290W construct that has a left-shifted G-V relationship and accelerated activation (Tao et al., 2010). However, when the *Shaker* S4 segment was mutated such that a lysine was at the top and an arginine at the bottom (i.e., *Shaker* R362K and K374R) and therefore more like that of hERG channels (i.e., K525 and R537; see Fig. 1), the F290W mutation slowed channel activation and stabilized the closed state (Tao et al., 2010). Thus, the behavior of the hERG F463W mutant described in Figs. 2 and 3 suggests a role for F463 in hERG that is similar to that described for F290 in *Shaker*.

### Effects of charge conserving mutations at the outer and inner bounds of S4

We next examined the possibility that the reversal of the lysine and arginine residues at the extremes of the S4 segment (see Fig. 1) contributes to the differences in gating between hERG and *Shaker* channels. Thus, the effects of the charge conserving hERG K525R, and R537K mutations were assessed (Fig. 4). K525R had a left-shifted G-V relationship (Fig. 4 B) and a large, negative $\Delta\Delta G_0$ (Table 1), which is indicative of a destabilized closed state relative to the open state. This is consistent with previous findings in both hERG (Subbiah et al., 2004, 2005; Zhang et al.,

TABLE 1

*Effects of mutations in S2 and S4 on voltage-dependent gating of hERG*

| Construct | 537/538[a] | $V_{1/2}$[b] | $k$[b] | $\Delta G_0$[c] | $\Delta\Delta G_0$[d,e] | $n$ | Stabilized state[f] | $\Delta\Delta G_{0,NA}$[g] |
|---|---|---|---|---|---|---|---|---|
| | | *mV* | *mV* | *kJ mol$^{-1}$* | *kJ mol$^{-1}$* | | | *kJ mol$^{-1}$* |
| WT (2 s) | RK | −27.7 ± 1.1 | 8.2 ± 0.1 | −8.4 ± 0.4 | NA | 13 | NA | NA |
| WT (10 s) | RK | −33.9 ± 1.2 | 7.5 ± 0.2 | −10.5 ± 1.0 | NA | 13 | NA | NA |
| WT (15 s) | RK | −35.1 ± 1.2 | 7.3 ± 0.2 | −12.1 ± 0.7 | NA | 13 | NA | NA |
| F463M | RK | −33.6 ± 2.3 | 9.7 ± 0.8 | −8.8 ± 1.2 | −0.4 ± 1.2 | 5 | NA | NA |
| F463W | RK | −7.1 ± 2.8 | 10.6 ± 0.6 | −1.6 ± 0.6 | 10.5 ± 0.9 | 7 | C | NA |
| F463L | RK | −21.3 ± 1.5 | 8.3 ± 0.3 | −6.3 ± 0.5 | 2.1 ± 0.7 | 6 | NA | NA |
| F463Y | RK | 12.2 ± 1.3 | 6.2 ± 0.3 | −4.8 ± 0.3 | 16.9 ± 0.8 | 4 | C | NA |
| F463V | RK | −23.1 ± 2.2 | 10.5 ± 0.9 | −5.9 ± 1.0 | 2.5 ± 1.1 | 8 | NA | NA |
| K525R | RK | −76.5 ± 3.3 | 8.5 ± 0.4 | −22.5 ± 18 | −14.1 ± 1.9 | 8 | O | NA |
| R537K | KK | −10.1 ± 1.3 | 9.7 ± 0.4 | −2.6 ± 0.4 | 5.8 ± 0.6 | 9 | C | NA |
| R537Q | QK | −16.6 ± 0.7 | 9.1 ± 0.3 | −4.5 ± 0.2 | 3.9 ± 0.5 | 7 | NA | NA |
| K538R | RR | 9.2 ± 1.4 | 8.3 ± 0.1 | 2.7 ± 0.4 | 13.2 ± 1.1 | 7 | C | NA |
| R537Q/K538R | QR | −10.2 ± 0.9 | 8.6 ± 0.7 | −3.0 ± 0.4 | 7.4 ± 1.1 | 7 | C | 11.7 ± 1.1 |
| R537K/K538R | KR | −3.1 ± 2.2 | 8.9 ± 0.3 | −0.9 ± 0.6 | 9.5 ± 1.2 | 6 | C | 11.5 ± 1.3 |
| K538Q | RQ | −65.6 ± 1.6 | 6.1 ± 0.1 | −26.5 ± 0.7 | −18.1 ± 0.9 | 5 | O | NA |
| R537K/K538Q | KQ | −49.0 ± 0.8 | 7.1 ± 0.2 | −17.1 ± 0.8 | −8.7 ± 0.9 | 8 | O | 3.6 ± 1.2 |
| R537Q/K538Q | QQ | −49.7 ± 1.8 | 6.8 ± 0.2 | −17.7 ± 0.9 | −9.3 ± 1.0 | 6 | O | 4.9 ± 1.3 |
| D466E | RK | −27.5 ± 2.0 | 10.5 ± 1.3 | −6.8 ± 1.0 | 1.6 ± 1.1 | 5 | NA | NA |
| D466E/K525R | RK | −34.3 ± 1.1 | 13.4 ± 0.3 | −6.3 ± 0.1 | 2.1 ± 0.5 | 6 | NA | 14.7 ± 2.1 |
| D466E/R537K | KK | 9.6 ± 1.2 | 15.7 ± 0.5 | 1.5 ± 0.2 | 9.9 ± 0.5 | 7 | C | 2.6 ± 1.2 |
| D466E/K538R | RR | −12.5 ± 1.1 | 10.2 ± 0.6 | −3.1 ± 0.5 | 7.3 ± 1.1 | 7 | C | 9.5 ± 1.5 |
| K525Q | RK | −116.0 ± 2.2 | 16.1 ± 0.9 | −18.0 ± 0.8 | −9.6 ± 0.9 | 9 | O | NA |
| D466E/K525Q | RK | −47.0 ± 1.5 | 11.6 ± 0.5 | −10.1 ± 0.5 | −1.7 ± 0.9 | 12 | NA | 10.1 ± 1.4 |
| F463W/K525R | RK | 13.7 ± 1.3 | 16.3 ± 1.1 | 2.1 ± 0.1 | 14.1 ± 0.7 | 5 | C | 14.1 ± 2.0 |
| F463W/R537K | KK | 8.3 ± 1.2 | 11.9 ± 0.2 | 1.7 ± 0.2 | 13.8 ± 0.7 | 5 | C | 6.2 ± 1.0 |
| F463W/K538R | RR | 17.0 ± 2.5 | 15.4 ± 0.3 | 2.7 ± 0.4 | 14.8 ± 0.7 | 8 | C | 10.5 ± 1.1 |

Superscripted numerals above each parameter refer to the equation used to calculate the parameter (see Materials and methods). Data are shown as means ± SEM. NA, not applicable.

[a]Letters denote the identities of the residues at positions 537 and 538.

[b]Eq. 1 was used to calculate the parameter.

[c]Eq. 2 was used to calculate the parameter.

[d]Eq. 3 was used to calculate the parameter.

[e]Eq. 4 was used to calculate the parameter.

[f]Defined as a $\Delta\Delta G_0 > |4.2|$ kJ mol$^{-1}$.

[g]Eq. 5 was used to calculate the parameter.

2004, 2005) and *Shaker* channels (Tao et al., 2010) that a lysine residue at the top of the S4 segment stabilizes the closed state. At the bottom of S4, R537K had a right-shifted G-V relationship and a positive $\Delta\Delta G_0$, which is suggestive of a relative stabilization of the closed state. This is counter to what would be predicted from work in *Shaker*; the analogous *Shaker* K374 residue favors the open conformation of that channel more than a substituted arginine (i.e., K374R; Tao et al., 2010). Given this finding, the imperfect alignment between the hERG and *Shaker* sequences (Cheng and Claydon, 2012), and the related uncertainty surrounding the structure of the base of the hERG S4 segment, the K538R mutant was also characterized. Intriguingly, compared with R537K, the hERG K538R mutant caused an even greater right-shift of the G-V relationship and a more positive $\Delta\Delta G_0$ (Fig. 4 B and Table 1).

Fig. 4 C compares the activation kinetics for the charge-conserving S4 mutations to those of WT hERG channels. K525R and R537K did not alter the time course of current activation over the range of electrochemical potentials tested. However, K538R increased $\tau_{act}$ (~5–10×), which is reminiscent of the effects of the F463W and F463Y mutants described in Fig. 3 C. Compared with the behavior of the R537K mutant, the increase in the relative stability of the closed state and slowing of activation by the K538R mutation are more in line with the findings from *Shaker* channels, and raise the question of which of the two basic residues, R537 or K538, is more important in hERG gating and the more appropriate functional homologue to *Shaker* K374. As observed with the F463 mutants, the effects of the S4 mutants on $\tau_{deact}$ were in contrast to their effects on $\tau_{act}$ (Fig. 4 D): K538R slowed deactivation, which seems counter to its drastic slowing of activation, whereas K525R and R537K accelerated deactivation despite leaving activation unchanged.

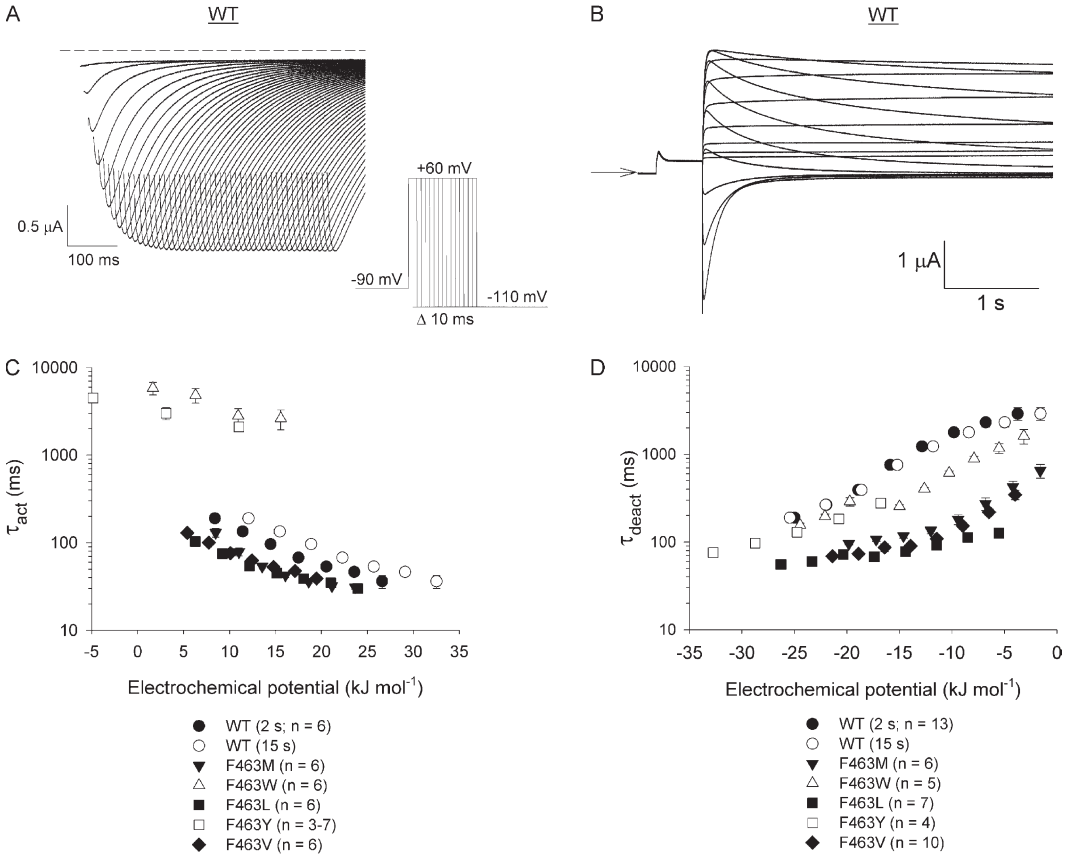


**Figure 3.** The F463W and F463Y mutations dramatically slow channel activation. (A) Typical WT hERG currents recorded during an envelope of tails voltage protocol (inset). For clarity, capacity transients have been removed and current traces truncated such that only the tail currents are shown. The broken line represents the zero current level. To measure $\tau_{act}$, peak tail current amplitudes were plotted against time and fit to a single exponential function. (B) Representative currents recorded from WT hERG channels during a deactivation protocol. Oocytes were held at −80 mV, depolarized to +60 mV for 500 ms to activate the channels, and then repolarized to potentials between −110 and +60 mV for 4 s. Tail currents were fit to a double exponential function and the value for $\tau_{deact}$ was calculated as a weighted mean of the fast and slow time constants for the current decay. (C and D) Plot of $\tau_{act}$ (C) and $\tau_{deact}$ (D) values for WT hERG and F463 mutant channels against the electrochemical potential for channel activation and deactivation, respectively (see Materials and methods). Because slower activating channels (e.g., F463W) were recorded using 15-s pulse durations, WT hERG data were plotted twice, using electrochemical potential energies calculated with $\Delta G_0$ values derived from G-V curves obtained using both 2- and 15-s pulse durations.

### Is R537 or K538 more important for hERG gating?

To define the relative roles and importance of R537 and K538 in hERG voltage-dependent gating, the effects of combining charge-neutralizing and/or charge-conserving mutations at both positions were examined. Fig. 5 (A–F) displays representative current traces recorded from oocytes expressing the six additional mutants tested (letters in parentheses denote the residues at 537 and 538; i.e., WT (RK)): R537Q (QK), R537Q/K538R (QR), R537K/K538R (KR), K538Q (RQ), R537K/K538Q (KQ), and R537Q/K538Q (QQ). The mean G-V relationships for these mutants are plotted in Fig. 5 (G–I), along with the Boltzmann fits describing those for WT (RK), R537K (KK), and K538R (RR). In agreement with earlier studies (Subbiah et al., 2004, 2005), we found that R537Q (QK) caused a slight right-shift of the G-V curve and small (<4.2 kJ mol$^{-1}$) $\Delta\Delta G_0$, whereas K538Q (RQ) caused a substantial hyperpolarizing shift of the G-V relationship and a related large, negative $\Delta\Delta G_0$ (Table 1). Because similar effects are observed with both neutral (R537Q) and charge-conserving (R537K) substitutions of 537 (Figs. 5, G and I; and Table 1), these results suggest that the relative stabilization of the closed state in R537K channels is unlikely to be caused by an altered electrostatic environment experienced by the residue at position 537. In contrast, the fact that K538A, K538Q, and K538D mutations (see Piper et al., 2005; Zhang et al., 2005) increase open state stability relative to the closed state while K538R (Fig. 4 B and Table 1) has the opposite effect is consistent with K538 being involved in electrostatic interactions important for stabilizing hERG channels in the closed state.

The relative importance of the residue at position 538 over that at 537 can be observed best by examining the effects of mutations at 537 when the identity of the residue at 538 is kept constant. This shows that as long as the identity of the residue at 538 was kept constant, both charge-conserving and charge-neutralizing substitutions of R537 had no effect on activation kinetics and elicited similar changes in the G-V relationships that were small compared with mutations of K538. First, as

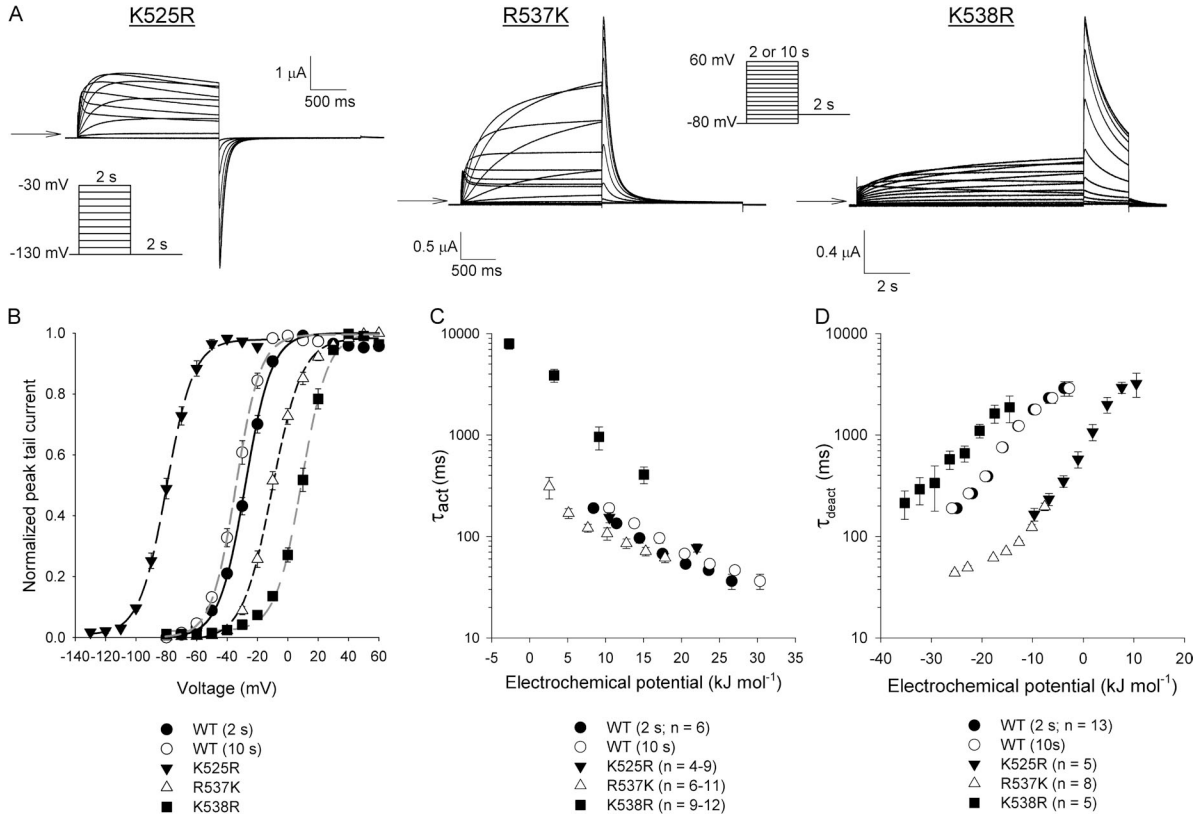


**Figure 4.** Charge-conserving mutations in S4 modulate hERG voltage-dependent gating. (A) Typical current traces recorded from S4 mutant channels in response to the voltage protocols shown (insets). Note the change in scale for K538R. Arrows indicate the zero current level. (B) Comparison of the mean G-V relationships for WT hERG and the mutant channels shown in A. Lines represent fits of the data to a Boltzmann function. ***n*** values and Boltzmann parameters are summarized in Table 1. (C) Plot of $\tau_{act}$ values for WT hERG and the S4 mutant channels against the electrochemical potential for activation. The envelope of tails protocol described in Fig. 3 A was used to measure $\tau_{act}$ values over a range of voltages that depended on the $V_{1/2}$ of the G-V curve for each mutant. (D) Comparison of $\tau_{deact}$ values for WT hERG and the S4 mutant channels. $\tau_{deact}$ was measured using the deactivation protocol described in Fig. 3 B, with a variable voltage range to accommodate the different shifts in the G-V curves caused by each mutant. For B–D, data points represent mean ± SEM (error bars). Similar to Fig. 3, electrochemical potential energies for WT hERG calculated using $\Delta G_0$ values derived from G-V curves obtained using both 2- and 10-s pulse durations are presented.

described in the previous paragraph, compared with the WT channel (RK), the R537K (KK) and R537Q (QK) mutations caused similar moderate right shifts of the G-V curves and $\Delta\Delta G_0$ values, which is indicative of closed state stabilization (Fig. 5 G and Tables 1 and 2). Second, the K538R (RR), R537K/K538R (KR), and R537Q/K538R (QR) double mutations all strongly right-shifted the G-V curve and stabilized the closed state (Fig. 5 H and Tables 1 and 2). Lastly, similar to the K538Q (RQ) mutation that left-shifted the G-V relationship and stabilized the open state, the R537K/K538Q (KQ) and R537Q/K538Q (QQ) mutants were also strongly left-shifted (Fig. 5 I and Tables 1 and 2). Additionally, the R537K/K538R (KR) and R537Q/K538R (QR) mutations had the very slow activation phenotype of K538R (RR), whereas the R537K (KQ) and R537Q/K538Q (QQ) double mutants

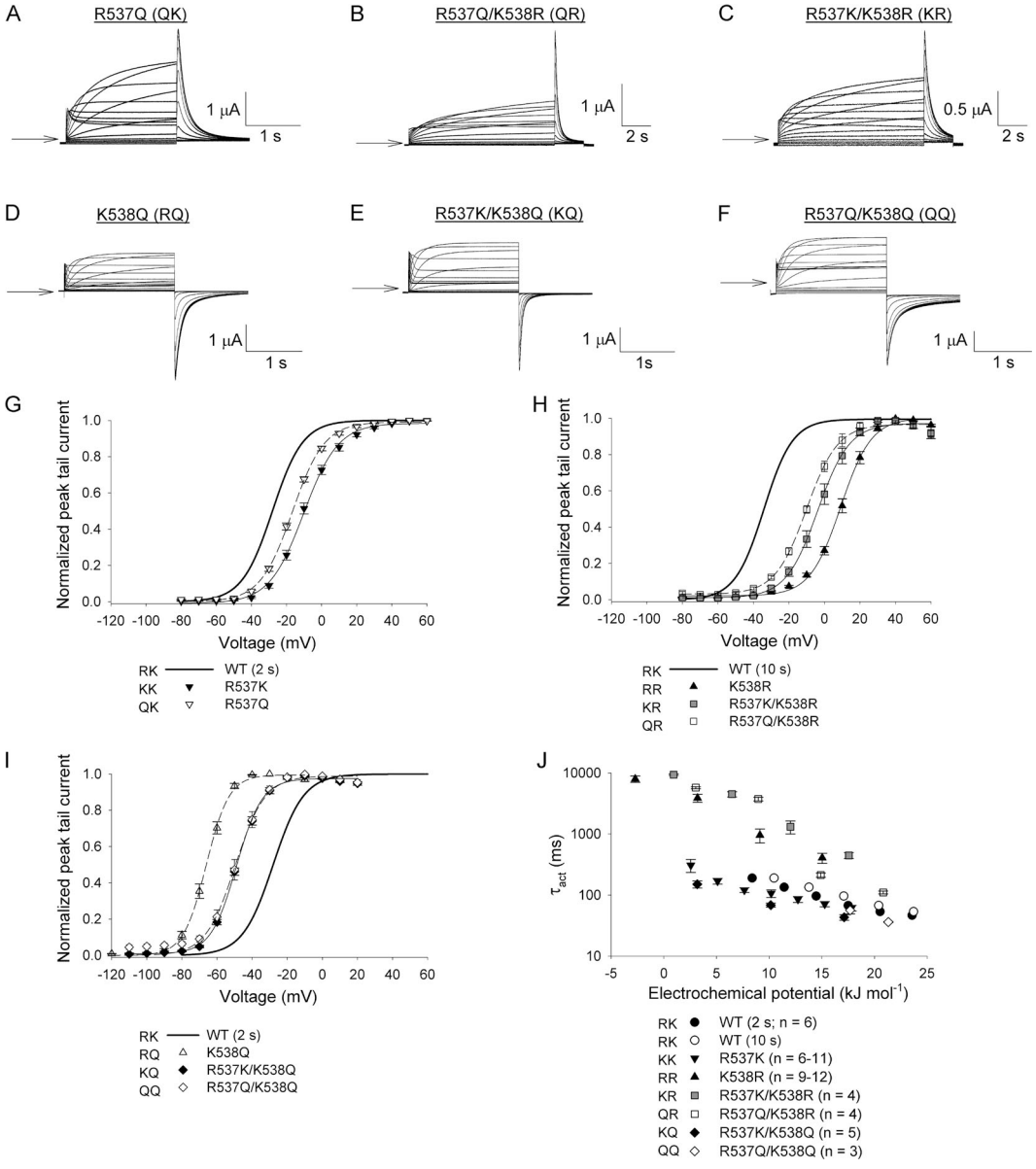


**Figure 5.** The positive charge at position 538 is more important than that at 537 in controlling channel activation. (A–F) Typical current recordings from oocytes expressing various R537 and K538 single and double mutations. Arrows represent the zero current level. (A–C) Oocytes were held at −80 mV and subjected to either 2-s (A) or 10-s (B and C) pulses to +60 mV in 10-mV increments; tail currents were recorded at −60 mV. (D–F) Oocytes were held at −130 mV and subjected to 2-s pulses to 0 or 20 mV in 10-mV increments; tail currents were recorded at −130 mV. (G) Comparison of the effects of R537 mutations (R/K/Q) on the G-V relationship when a Lys residue is present at position 538. (H) Comparison of the effects of R537 (R/K/Q) mutations when the residue at position 538 is an Arg. (I) Comparison of the effects of R537 mutations (R/K/Q) on the G-V relationship when a Q residue is present at position 538. Lines in G–I represent fits of the data to a Boltzmann function. ***n*** values and Boltzmann parameters are summarized in Table 1. (J) Plot of the $\tau_{act}$ values against the electrochemical potential for activation for the R537 and K538 double mutants. Data points in G–J represent mean ± SEM (error bars).

did not appear to affect activation kinetics over the range of electrochemical potentials tested (Fig. 5 J). In sum, the largest perturbations of activation kinetics and the relative stabilities of the closed and open state of hERG channels occurred with mutations at position 538 (Tables 1 and 2), which suggests that the native K538 residue may be a more important determinant of voltage-dependent gating than the neighboring R537.

To deduce whether the adjacent R537 and K538 residues influence each other, i.e., are functionally coupled, double mutant cycle analysis (Yifrach and MacKinnon, 2002; Zhang et al., 2005) was performed to calculate the degree of nonadditivity ($\Delta\Delta G_{0,NA}$) using $\Delta G_0$ values from both the single and double mutants (see Materials and methods). Coupling between two mutation sites is assumed if the effects of the mutations are not additive; that is, if the degree of nonadditivity exceeds the cut-off value of 4.2 kJ mol$^{-1}$ (Yifrach and MacKinnon, 2002; Zhang et al., 2005). The calculated $\Delta\Delta G_{0,NA}$ values for R537K/K538R (KR) and R537Q/K538R (QR) are >11 kJ mol$^{-1}$, whereas those for R537K/K538Q (KQ) and R537Q/K538Q (QQ) are 3.6 and 4.9 kJ mol$^{-1}$, respectively (Tables 1 and 2). Overall, these results suggest that the effects of mutations at positions 537 and 538 are not additive and imply that the positively charged residues at positions 537 and 538 are functionally coupled. Thus, R537 and K538 may affect each other's ability to regulate voltage-dependent gating, but, as suggested by the results presented in Fig. 5 and Tables 1 and 2, K538 appears to be dominant in the regulation of channel gating.

### Interaction of the S4 charges with F463W

We have shown that mutation of F463, as well as of K525 and K538, has strong effects on voltage-dependent gating of hERG channels. To determine whether interactions similar to those between F290 and S4 charges in *Shaker* channels also occur in hERG channels, the effects of combining the F463W and charge-conserving S4 mutations were examined. The G-V relationships of the F463W/K525R and F463W/K538R double mutants are displayed in Fig. 6 (A and B), alongside the relevant single mutations. Parameters for Boltzmann fits to the data are summarized in Table 1. Both double mutants had G-V relationships that were shallower and quite right-shifted relative to WT and the single F463W mutant channels. The $\Delta\Delta G_0$ values were large and positive (Table 1), which is consistent with a strong relative stabilization of the closed state. Also in agreement with closed state stabilization, the activation kinetics for the F463W/K525R and F463W/K538R were exceedingly slow and on par with those of the single F463W mutant (Fig. 6 D). Double mutant cycle analysis resulted in $\Delta\Delta G_{0,NA}$ values well in excess of 4.2 kJ mol$^{-1}$ for both F463W/K525R and F463W/K538R (Table 1), which strongly suggests that F463 is able to form functional interactions with both K525 and K538 during activation gating and is consistent with the possibility that F463 serves as a gating charge transfer center in hERG channels. In contrast, double mutant cycle analysis of the effects of the F463W/R537K double mutant on the G-V relationship (Fig. 6 C) resulted in a $\Delta\Delta G_{0,NA}$ of 6.2 ± 1.1 kJ mol$^{-1}$ (Table 1). Although this value suggests that R537 may be functionally coupled to F463, it is substantially lower than the $\Delta\Delta G_{0,NA}$ for F463W/K538R, which is consistent with our earlier conclusion (Fig. 5 and Table 2) that K538 is likely more important than R537 in the regulation of steady-state activation.

### Interaction of the S4 charges with D466 in S2

It has previously been suggested that S4 gating charges in *Shaker* channels interact not only with the conserved

TABLE 2

*Comparison of the effects of mutations at positions 537 and 538 on closed- and open-state stability*

| 537 | Parameter | 538 | | |
|---|---|---|---|---|
| | | R | K | Q |
| R | | **C** | **WT** | **O** |
| | $\Delta G_0$ | 2.7 | −8.4 (2 s), −10.5 (10 s) | −26.5 |
| | $\Delta\Delta G_0$ | 13.2 | | −18.1 |
| | $\Delta\Delta G_{0,NA}$ | | | |
| K | | **C** | **C** | **O** |
| | $\Delta G_0$ | −0.9 | −2.6 | −17.1 |
| | $\Delta\Delta G_0$ | 9.5 | 5.8 | −8.7 |
| | $\Delta\Delta G_{0,NA}$ | 11.5 | | 3.6 |
| Q | | **C** | **NA** | **O** |
| | $\Delta G_0$ | −3.0 | −4.5 | −17.7 |
| | $\Delta\Delta G_0$ | 7.4 | 3.9 | −9.3 |
| | $\Delta\Delta G_{0,NA}$ | 11.7 | | 4.9 |

Letters (C/O) within cells indicate whether the combination of residues at 537 (rows) and 538 (columns) resulted in a stabilization of the closed or open state, relative to WT hERG. For ease of comparison, the mean values for $\Delta G_0$, $\Delta\Delta G_0$, and $\Delta\Delta G_{0,NA}$ (in kJ mol$^{-1}$) are also shown. Refer to Table 1 for full details, including *n* values and SEM.

phenylalanine residue in the S2 segment, but also with negative residues in the S2 (E293) and S3 (D316) segments (Papazian et al., 1995; Tiwari-Woodruff et al., 1997; Tao et al., 2010). Although these negative charges are conserved in the hERG VSD, the analogous residue to *Shaker* E293 is hERG D466 (Fig. 1). We used the D466E mutation to assess whether this difference in the nature of the negative charge contributes to the unique properties of hERG channel gating. In addition, the D466E/K525R, D466E/R537K, and D466E/K538R double mutations were generated to test for functional interactions between these S2 and S4 residue pairs. Fig. 7 displays sample current traces from these mutants, as well as comparisons of their G-V relationships with those of the WT and the single S4 charge-conserving mutant channels. The D466E mutation alone had no effect on the G-V relationship (Fig. 7 E and Table 1). However, the D466E/K525R mutation exhibited a dramatic phenotype: the left-shifted G-V relationship of K525R was largely reversed by the D466E mutation, such that the double mutant G-V relationship was similar to those of WT and D466E channels (Fig. 7 E and Table 1). This suggests that in the background of the K525R mutation, which causes a relative destabilization of the closed state and left-shifts the G-V curve, a substituted glutamate residue at position 466 is able to restore closed state stability and rescue WT-like gating. Indeed, double mutant cycle analysis for the D466E/K525R mutant results in a $\Delta\Delta G_{0,NA}$ value of $\sim$15 kJ mol$^{-1}$ (Table 1), which strongly implies that there is a functional interaction between the residues at these two positions. To determine whether this interaction is electrostatic in nature, we also tested the D466E/K525Q double mutant. As shown in Fig. 7 F, the D466E mutation largely rescues the WT-like G-V relationship in the otherwise strongly hyperpolarized K525Q background; the D466E/K525Q mutant has a $\Delta\Delta G_{0,NA}$ value of $\sim$10 kJ mol$^{-1}$. The similar results observed with both charge-conserving and charge-neutralizing mutations at position 525 suggest that the interaction between the residues at positions 466 and 525 is not electrostatic in nature. In the case of the D466E/K538R double mutant, activation kinetics were very slow, similar to those of the K538R single mutation (Fig. 7 D), and the G-V relationship revealed a $V_{1/2}$ that was intermediate between that of WT and K538R channels (Fig. 7 H). The $\Delta\Delta G_{0,NA}$ value for this pairing was $\sim$10 kJ mol$^{-1}$ (Table 1), which suggests that D466 can also form functional interactions with K538. In contrast to the results with D466E/K525R and D466E/K538R, double mutant cycle analysis of the effects of the D466E/R537K on the G-V relationship gave a $\Delta\Delta G_{0,NA}$ $\sim$3 kJ mol$^{-1}$ (Fig. 7 G and Table 1), which indicates that D466 does not interact with R537 and is again consistent with our conclusion that, relative to K538, R537 has a less dominant

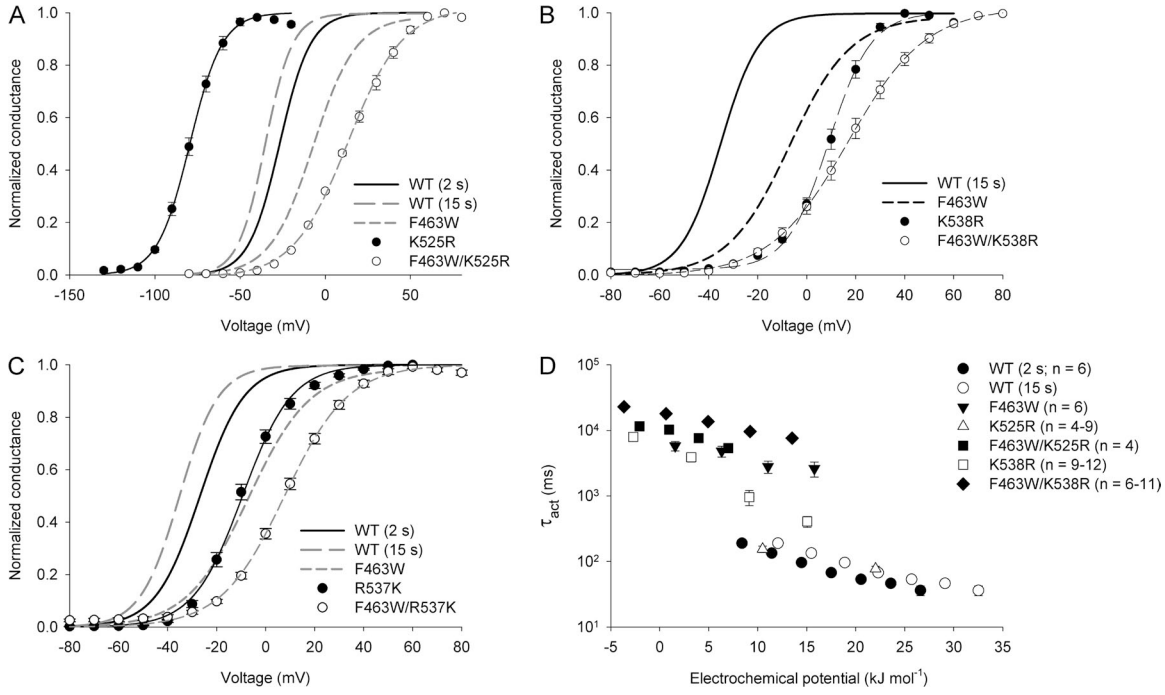


**Figure 6.** F463 may interact with K525 and K538 to modulate activation gating. (A) Comparison of the mean G-V relationship for the F463W/K525R double mutation with those of the single mutants. (B) Comparison of the mean G-V relationships for the F463W/K538R double mutation with those of the single mutants. (C) Comparison of the G-V relationships for the F463W/R537K double mutation with those of the single mutants. Lines in A–C represent Boltzmann function descriptions of the data; *n* values and Boltzmann parameters are shown in Table 1. (D) Plot of the $\tau_{act}$ values against the electrochemical potential for activation for the channel constructs described in A and B. Data points represent mean ± SEM (error bars).

role in the regulation of voltage-dependent gating. Collectively the data in Fig. 7 suggest that D466 forms functional interactions with K525 at the top of S4 and K538 at the bottom. These interactions appear not to be electrostatic in nature, but are dependent on the specific identity of the charged residues at positions 466, 525, and 538.

## DISCUSSION

It has been suggested that S4 movement in Kv1 family channels may be regulated by conserved hydrophobic and acidic residues in the S2 segment (Tao et al., 2010; Lacroix and Bezanilla, 2011; Henrion et al., 2012). Consistent with results in *Shaker* channels (Tao et al., 2010), we found that substitution of F463 with the bulky, hydrophobic Trp residue right-shifted the steady-state G-V relationship (Fig. 2 B) and dramatically slowed channel activation (Fig. 3 C), which is indicative of a stabilization of the closed state. We also showed that the relative stabilities of the closed and open states of the hERG channel were greater when the positively charged residue at the outer (K525) and inner (K538) ends of the S4 segment, respectively, was a Lys rather than an Arg (Fig. 4). Lastly, the results of double mutant cycle analysis suggested that the K525 and K538 residues form strong functional interactions with F463 (Fig. 6) and with D466 in S2 (Fig. 7), which have been proposed to contribute to formation of a gating charge transfer center in *Shaker* channels (Tao et al., 2010). Together, these data support the hypothesis that a similar gating charge transfer center mediates movement of the S4 voltage sensor in hERG channels.

### A Lys residue at the outer and inner ends of S4 stabilizes hERG resting and activated states, respectively

It has been shown in *Shaker* channels that a substituted Trp residue at position 290 preferentially interacted

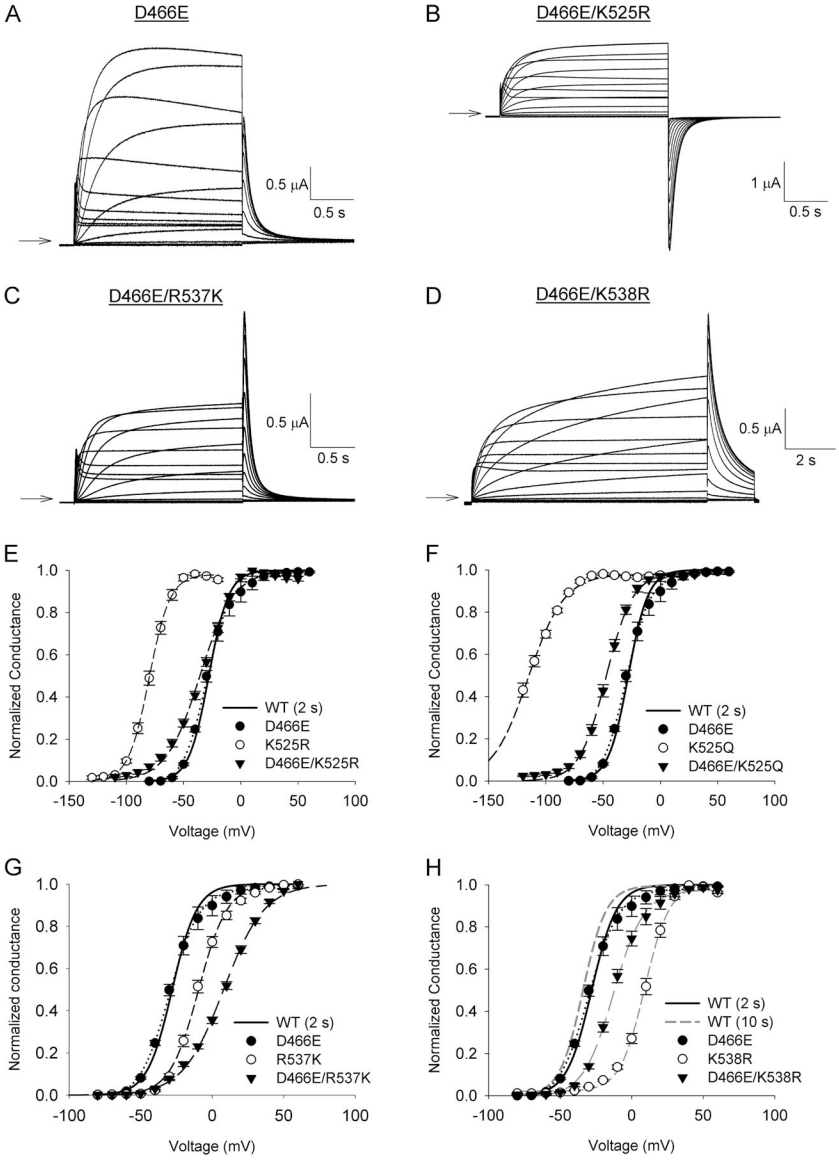


**Figure 7.** K525 and K538 may interact with a conserved negative charge in S2. (A–D) Representative current traces from oocytes expressing the single D466E mutation and the double D466E/K525R, D466E/R537K, or D466E/K538R mutant constructs. Oocytes were held at −80 mV and subjected to either 2- or 10-s depolarizing pulses to +60 mV in 10-mV increments. Tail currents were recorded at −60 mV. Arrows indicate the zero current level. The exception to this was D466E/K525R, which was held at −110 mV, and tail currents were recorded at −130 mV. (E) Comparison of the G-V relationships for the D466E and D466E/K525R mutants. (F) Plot of the G-V relationships for the D466E and D466E/K525Q mutants. (G) Comparison of the G-V relationships for the D466E and D466E/R537K mutants. (H) Comparison of the G-V relationships for the D466E and D466E/K538R mutants. In E–H, lines represent fits of the data to a Boltzmann function. Data points represent mean ± SEM (error bars). *n* values and parameters from the Boltzmann fits are summarized in Table 1.

with Lys over Arg residues, such that a relative stabilization of the resting or activated conformations of the voltage sensor occurred depending on whether a Lys occupied the first (i.e., R362K, R1K) or fifth (i.e., K374, K5) charged position in S4, respectively (Tao et al., 2010). Consistent with these findings, we found that the native K525 residue at the top of the S4 segment in hERG stabilizes the closed state of the channel compared with when an Arg residue is substituted at this position (Fig. 4). We (Figs. 7, E and F; and Table 1) and others (Subbiah et al., 2004, 2005; Zhang et al., 2004, 2005; Subbotina et al., 2010) have also shown that the stabilization of the closed state by K525 is likely not dependent on charge, as substitutions with neutral (Gln, Cys, Trp) or acidic (Asp, Glu) residues also left-shift the G-V relationship. It is worth noting that we have used an alignment that places K525 in the equivalent position to R362 (R1), rather than R365 (R2) in *Shaker* (Fig. 1), based on S4 accessibility studies in hERG (Elliott et al., 2009) and the observation that despite some uncertainty as to the alignment between the S4 segments of the hERG, *Shaker*, and Kv1.2 channels (Subbiah et al., 2004; Zhang et al., 2004; Piper et al., 2005; Elliott et al., 2009; Es-Salah-Lamoureux et al., 2010; Cheng and Claydon, 2012), molecular dynamics simulations of hERG (Subbotina et al., 2010; Durdagi et al., 2012) suggest that K538 is located at the base of the S4 segment and not in the S4–S5 linker, regardless of which of the two most popular S4 alignments were used.

We show that the native K538 residue is better able to stabilize the open state of the channel than a substituted Arg residue, which right-shifts the G-V curve and dramatically increases $\tau_{act}$ (Fig. 4); this result is consistent with the suggestion in *Shaker* channels that K374 at the bottom of S4 stabilizes the activated conformation of the voltage sensor (Tao et al., 2010). The fact that the K538Q (Fig. 5 and Table 1), -A, -C, -W, and -D mutations (Piper et al., 2005; Subbiah et al., 2005; Zhang et al., 2005) cause hyperpolarizing shifts of the G-V relationship and decreases in $\tau_{act}$, whereas K538R has the opposite effects (Fig. 4), suggests that K538, unlike K525, may also be involved in electrostatic interactions important for stabilizing hERG channels in the closed state. It has been suggested that K538 interacts electrostatically with D411 in S1 to stabilize a transition state early in the activation pathway (Zhang et al., 2005), such that disruption of this interaction (e.g., with the D411K or K538D mutations) eases transition to late activation states. The stabilization of the closed state associated with the K538R mutation may therefore be caused by a strengthening of this interaction by the substituted Arg residue. Perhaps Arg residues at this site retain their charge better than Lys residues, which can show altered pKa values and, thus ionization, depending on how the residue is buried within the channel protein (Harms et al., 2011; Isom et al., 2011).

### K538 is the dominant positively charged residue at the base of the hERG S4

Using charge-conserving and -neutralizing mutations, we found that K538 had a greater influence on channel activation than the adjacent R537 residue (Fig. 5 and Table 2). This conclusion was supported by the results of double mutant cycle analysis, which strongly suggested that K538 can interact with both F463 and D466 to modulate voltage-dependent gating, whereas R537 may interact only weakly with F463W and not at all with D466 (Figs. 6 and 7; and Table 1). Importantly, the dominant role of K538 does not imply that R537 does not affect hERG gating; mutation of R537 alone can modulate voltage dependence, and double mutant cycle analysis showed that R537 and K538 are energetically coupled (Fig. 5 and Tables 1 and 2). Thus, although R537 may not strongly interact with F463 or D466 directly, it may influence the nature of the interaction of K538 with these S2 residues. The presence of two adjacent basic residues at the base of the hERG S4 segment and their combined influence on gating is in contrast to the situation in *Shaker*-type channels, which have only the single Lys residue in the homologous position, and likely contributes to the different gating behaviors in the two channels.

### hERG S4 mutations affect both steady-state activation and gating kinetics

A major difference between our findings and those reported in *Shaker* (Tao et al., 2010) are that the effects of the hERG mutations on steady-state activation and gating kinetics often cannot be explained by the simple five-state model of voltage sensor transitions proposed for *Shaker*. Each state in that model described the conformation of a single voltage sensor as the positively charged residues (i.e., R1 – K5) moved sequentially into position to interact with F290. Correspondingly, the ability of mutations at R1 or K5 to affect steady-state stabilities and activation or deactivation kinetics could be described by changing the relative energy of the first or fifth states, respectively (Tao et al., 2010). This model cannot explain how the hERG K525R mutation at the top of S4, which would be expected to affect early transitions and activation kinetics, had no effect on $\tau_{act}$ and instead stabilized the open state and accelerated deactivation, effects that imply a change in the final closed-to-open transition.

To describe the effects of the K525R and K538R mutations on hERG gating, we used a simple linear kinetic model (Fig. 8) first proposed by Wang et al. (1997) and based on ionic current data. The model is comprised of three closed states preceding a final open state (inactivation has been omitted for simplicity). The transitions along the activation pathway are depicted in a reaction coordinate diagram: each state occupies an energy well, and transition rates depend on the height of the connecting energy barriers. The effects of the K525R mutation (open state stabilization, faster deactivation; Fig. 8 A) were most

simply satisfied by increasing the relative depth of the energy well for the O state and decreasing the energy barrier for the O → $C_2$ transition. Activation kinetics are unaffected, as the energy barrier for the rate limiting forward transition ($E_{(act)}$) does not change. The effects of the K538R mutation can also be described using this scheme (Fig. 8 B): the stabilization of the closed state and increase in both $\tau_{act}$ and $\tau_{deact}$ may all be achieved by increasing the height of the energy barrier between $C_2$ and O and decreasing the depth of the energy well for the O state. Overall, the model is limited in that the transitions do not correlate to the movement of individual S4 gating charges and thus provides little mechanistic insight into S4 movement, in contrast to the more complex schemes used for *Shaker* channels (e.g., Zagotta et al., 1994; Schoppa and Sigworth, 1998; Tao et al., 2010) that incorporate gating current data. Nevertheless, Fig. 8 helps to illustrate possible energetic explanations for how the mutations may concomitantly affect steady-state activation and gating kinetics.

### What is the nature of the interactions between F463, D466, and S4 gating charges in hERG?

The major finding presented here is that F463 and D466 in the hERG S2 segment interact with K525 in the resting state and K538 in the activated state to regulate voltage-dependent gating (Fig. 8 C). These results are consistent with the behavior of the gating charge transfer center proposed for *Shaker* channels (Tao et al., 2010; Pless et al., 2011). That K525 interacts with F463 and D466 is also in agreement with the results of Lin et al. (2011), who showed that R362 at the top of the *Shaker* S4 segment occupies the gating charge transfer center in the resting state. An outstanding question here is how mutation of K525 at the top of the S4 segment can cause the perturbation to the transition between the last preopen closed state and the open state suggested in Fig. 8 A, because in *Shaker* channels the analogous mutation would be expected to perturb the first transition in the activation pathway. Furthermore, there is other evidence from our macroscopic ionic current recordings to suggest that the nature of the interactions in hERG channels differs from those described in *Shaker*. First, the effects of the hERG F463Y, -L, -M, and -V mutations on the G-V curve differed from those of the analogous mutations of F290 in *Shaker* (Tao et al., 2010; Lacroix and Bezanilla, 2011). Second, hERG K525R and K538R accelerated and decelerated deactivation kinetics, respectively, whereas the analogous mutations in *Shaker* had either no effect or

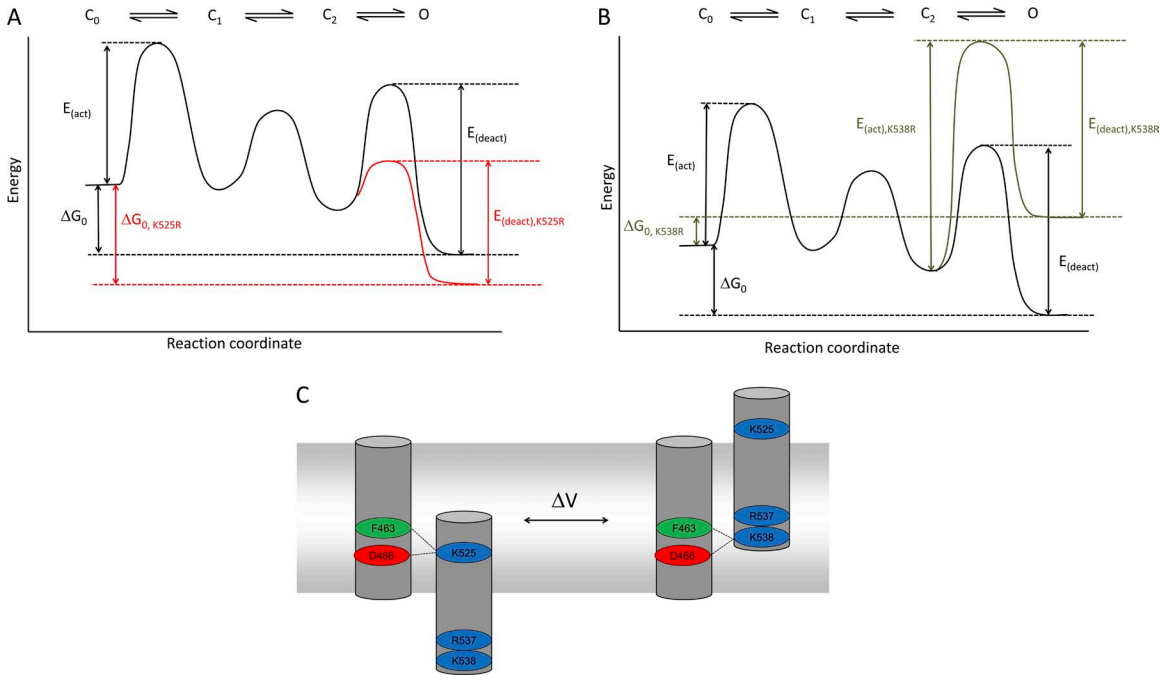


**Figure 8.** Schematic representation of hERG channel gating. (A) Reaction coordinate diagram for hERG gating, based on the linear gating scheme proposed by Wang et al. (1997). Activation involves transitions through three closed (C) states to a single open (O) state; the inactivated state has been omitted for simplicity. The black line represents the gating reaction for WT channels; the red line highlights possible changes caused by the K525R mutation. These include a more negative value for $\Delta G_0$ consistent with stabilization of the O state and a decrease in the energy barrier ($E_{(deact)}$) for the O → $C_2$ transition to allow for faster deactivation. (B) The same reaction coordinate diagram in A is used to highlight the possible changes to the gating reaction caused by the K538R mutation (green line). These include a positive value for $\Delta G_0$ consistent with stabilization of the closed state and a large increase in the energy barriers for transitions between the $C_2$ and O states that allows for the increases in the values of $\tau_{act}$ and $\tau_{deact}$. (C) Schematic showing the proposed functional interactions between the S4 gating charges and F463 and D466 in the S2 segment. Broken lines illustrate the interaction pairs thought to occur in the resting state (left) and the activated state (right).

accelerated deactivation, respectively (Tao et al., 2010). Third, the F463W mutation in hERG did not exaggerate the shifts in the G-V curve caused by the K525R or K538R mutations (Fig. 6), in contrast to *Shaker* F290W, which formed a preferential cation–π interaction with Lys over Arg residues (Tao et al., 2010; Pless et al., 2011). This implies that the interactions between F463W and Lys residues in the hERG S4 segment are unlikely to involve cation–π forces. Fourth, based on gating current measurements, F290 only regulates movement of the fourth charged residue in the *Shaker* S4 segment (Lacroix and Bezanilla, 2011), whereas we present evidence of an interaction between F463 and K525 at the top of the hERG S4 (Fig. 6). These differences may be caused by variations in structure–function relationships in hERG and *Shaker* channels, including but not limited to the putative interaction between R537 and K538 at the base of the hERG S4 segment (Fig. 5), the presence in the hERG voltage sensing domain of three additional acidic residues that may modulate activation by interacting with S4 charges (Liu et al., 2003; Zhang et al., 2005), and the additional regulation of hERG by internal cytosolic domains (Wynia-Smith et al., 2008; Gustina and Trudeau, 2011; Ng et al., 2012; Tan et al., 2012). Elucidating the physical nature of the interactions between F463, D466, K525, and K538 will require further investigation to directly monitor voltage sensor dynamics.

This study was supported by a Grant-in-aid from the Heart and Stroke Foundation of British Columbia and Yukon (T.W. Claydon), a Natural Sciences and Engineering Research Council of Canada Discovery grant (T.W. Claydon), and support from the Canada Foundation for Innovation Leader's Opportunity Fund (T.W. Claydon). T.W. Claydon was supported by a Heart and Stroke New Investigator Award and a Michael Smith Foundation for Health Research Career Scholar Award. Y.M. Cheng was supported by a Research Fellowship from the Heart and Stroke Foundation of Canada. C.M. Niven was supported by a Natural Sciences and Engineering Research Council Undergraduate Research Student Award.

Kenton J. Swartz served as editor.

Submitted: 15 March 2013
Accepted: 2 August 2013

## REFERENCES

Ahern, C.A., and R. Horn. 2005. Focused electric field across the voltage sensor of potassium channels. *Neuron.* 48:25–29. http://dx.doi.org/10.1016/j.neuron.2005.08.020

Chen, X., Q. Wang, F. Ni, and J. Ma. 2010. Structure of the full-length Shaker potassium channel Kv1.2 by normal-mode-based X-ray crystallographic refinement. *Proc. Natl. Acad. Sci. USA.* 107:11352–11357. http://dx.doi.org/10.1073/pnas.1000142107

Cheng, Y.M., and T.W. Claydon. 2012. Voltage-dependent gating of HERG potassium channels. *Front. Pharmacol.* 3:83. http://dx.doi.org/10.3389/fphar.2012.00083

Chowdhury, S., and B. Chanda. 2012. Estimating the voltage-dependent free energy change of ion channels using the median voltage for activation. *J. Gen. Physiol.* 139:3–17. http://dx.doi.org/10.1085/jgp.201110722

Curran, M.E., I. Splawski, K.W. Timothy, G.M. Vincent, E.D. Green, and M.T. Keating. 1995. A molecular basis for cardiac arrhythmia: HERG mutations cause long QT syndrome. *Cell.* 80:795–803. http://dx.doi.org/10.1016/0092-8674(95)90358-5

Durdagi, S., S. Deshpande, H.J. Duff, and S.Y. Noskov. 2012. Modeling of open, closed, and open-inactivated states of the hERG1 channel: structural mechanisms of the state-dependent drug binding. *J. Chem. Inf. Model.* 52:2760–2774. http://dx.doi.org/10.1021/ci300353u

Elliott, D.J., N.Y. Dondas, T.S. Munsey, and A. Sivaprasadarao. 2009. Movement of the S4 segment in the hERG potassium channel during membrane depolarization. *Mol. Membr. Biol.* 26:435–447. http://dx.doi.org/10.3109/09687680903321081

Es-Salah-Lamoureux, Z., R. Fougere, P.Y. Xiong, G.A. Robertson, and D. Fedida. 2010. Fluorescence-tracking of activation gating in human ERG channels reveals rapid S4 movement and slow pore opening. *PLoS ONE.* 5:e10876. http://dx.doi.org/10.1371/journal.pone.0010876

Gustina, A.S., and M.C. Trudeau. 2011. hERG potassium channel gating is mediated by N- and C-terminal region interactions. *J. Gen. Physiol.* 137:315–325. http://dx.doi.org/10.1085/jgp.201010582

Harms, M.J., J.L. Schlessman, G.R. Sue, and B. García-Moreno. 2011. Arginine residues at internal positions in a protein are always charged. *Proc. Natl. Acad. Sci. USA.* 108:18954–18959. http://dx.doi.org/10.1073/pnas.1104808108

Henrion, U., J. Renhorn, S.I. Börjesson, E.M. Nelson, C.S. Schwaiger, P. Bjelkmar, B. Wallner, E. Lindahl, and F. Elinder. 2012. Tracking a complete voltage-sensor cycle with metal-ion bridges. *Proc. Natl. Acad. Sci. USA.* 109:8552–8557. http://dx.doi.org/10.1073/pnas.1116938109

Isom, D.G., C.A. Castañeda, B.R. Cannon, and B. García-Moreno. 2011. Large shifts in pKa values of lysine residues buried inside a protein. *Proc. Natl. Acad. Sci. USA.* 108:5260–5265. http://dx.doi.org/10.1073/pnas.1010750108

Jiang, Y., A. Lee, J. Chen, V. Ruta, M. Cadene, B.T. Chait, and R. MacKinnon. 2003. X-ray structure of a voltage-dependent $K^+$ channel. *Nature.* 423:33–41. http://dx.doi.org/10.1038/nature01580

Lacroix, J.J., and F. Bezanilla. 2011. Control of a final gating charge transition by a hydrophobic residue in the S2 segment of a $K^+$ channel voltage sensor. *Proc. Natl. Acad. Sci. USA.* 108:6444–6449. http://dx.doi.org/10.1073/pnas.1103397108

Liman, E.R., P. Hess, F. Weaver, and G. Koren. 1991. Voltage-sensing residues in the S4 region of a mammalian $K^+$ channel. *Nature.* 353:752–756. http://dx.doi.org/10.1038/353752a0

Lin, M.C., J.Y. Hsieh, A.F. Mock, and D.M. Papazian. 2011. R1 in the *Shaker* S4 occupies the gating charge transfer center in the resting state. *J. Gen. Physiol.* 138:155–163. http://dx.doi.org/10.1085/jgp.201110642

Liu, J., M. Zhang, M. Jiang, and G.N. Tseng. 2003. Negative charges in the transmembrane domains of the HERG K channel are involved in the activation- and deactivation-gating processes. *J. Gen. Physiol.* 121:599–614. http://dx.doi.org/10.1085/jgp.200308788

Li-Smerin, Y., D.H. Hackos, and K.J. Swartz. 2000. α-helical structural elements within the voltage-sensing domains of a $K(^+)$ channel. *J. Gen. Physiol.* 115:33–50. http://dx.doi.org/10.1085/jgp.115.1.33

Long, S.B., E.B. Campbell, and R. Mackinnon. 2005. Crystal structure of a mammalian voltage-dependent *Shaker* family $K^+$ channel. *Science.* 309:897–903. http://dx.doi.org/10.1126/science.1116269

Long, S.B., X. Tao, E.B. Campbell, and R. MacKinnon. 2007. Atomic structure of a voltage-dependent $K^+$ channel in a lipid membrane-like environment. *Nature.* 450:376–382. http://dx.doi.org/10.1038/nature06265

Lu, Z., A.M. Klem, and Y. Ramu. 2002. Coupling between voltage sensors and activation gate in voltage-gated $K^+$ channels. *J. Gen. Physiol.* 120:663–676. http://dx.doi.org/10.1085/jgp.20028696

Ng, C.A., M.D. Perry, P.S. Tan, A.P. Hill, P.W. Kuchel, and J.I. Vandenberg. 2012. The S4-S5 linker acts as a signal integrator for HERG K+ channel activation and deactivation gating. *PLoS ONE*. 7:e31640. http://dx.doi.org/10.1371/journal.pone.0031640

Papazian, D.M., L.C. Timpe, Y.N. Jan, and L.Y. Jan. 1991. Alteration of voltage-dependence of Shaker potassium channel by mutations in the S4 sequence. *Nature*. 349:305–310. http://dx.doi.org/10.1038/349305a0

Papazian, D.M., X.M. Shao, S.A. Seoh, A.F. Mock, Y. Huang, and D.H. Wainstock. 1995. Electrostatic interactions of S4 voltage sensor in Shaker $K^+$ channel. *Neuron*. 14:1293–1301. http://dx.doi.org/10.1016/0896-6273(95)90276-7

Piper, D.R., W.A. Hinz, C.K. Tallurri, M.C. Sanguinetti, and M. Tristani-Firouzi. 2005. Regional specificity of human ether-a'-go-go-related gene channel activation and inactivation gating. *J. Biol. Chem.* 280:7206–7217. http://dx.doi.org/10.1074/jbc.M411042200

Piper, D.R., J. Rupp, F.B. Sachse, M.C. Sanguinetti, and M. Tristani-Firouzi. 2008. Cooperative interactions between R531 and acidic residues in the voltage sensing module of hERG1 channels. *Cell. Physiol. Biochem.* 21:37–46. http://dx.doi.org/10.1159/000113745

Pless, S.A., J.D. Galpin, A.P. Niciforovic, and C.A. Ahern. 2011. Contributions of counter-charge in a potassium channel voltage-sensor domain. *Nat. Chem. Biol.* 7:617–623. http://dx.doi.org/10.1038/nchembio.622

Sanguinetti, M.C., and N.K. Jurkiewicz. 1990. Two components of cardiac delayed rectifier $K^+$ current. Differential sensitivity to block by class III antiarrhythmic agents. *J. Gen. Physiol.* 96:195–215. http://dx.doi.org/10.1085/jgp.96.1.195

Sanguinetti, M.C., and M. Tristani-Firouzi. 2006. hERG potassium channels and cardiac arrhythmia. *Nature*. 440:463–469. http://dx.doi.org/10.1038/nature04710

Sanguinetti, M.C., C. Jiang, M.E. Curran, and M.T. Keating. 1995. A mechanistic link between an inherited and an acquired cardiac arrhythmia: HERG encodes the $I_{Kr}$ potassium channel. *Cell*. 81:299–307. http://dx.doi.org/10.1016/0092-8674(95)90340-2

Schönherr, R., B. Rosati, S. Hehl, V.G. Rao, A. Arcangeli, M. Olivotto, S.H. Heinemann, and E. Wanke. 1999. Functional role of the slow activation property of ERG $K^+$ channels. *Eur. J. Neurosci.* 11:753–760. http://dx.doi.org/10.1046/j.1460-9568.1999.00493.x

Schoppa, N.E., and F.J. Sigworth. 1998. Activation of *Shaker* potassium channels. III. An activation gating model for wild-type and V2 mutant channels. *J. Gen. Physiol.* 111:313–342. http://dx.doi.org/10.1085/jgp.111.2.313

Starace, D.M., and F. Bezanilla. 2004. A proton pore in a potassium channel voltage sensor reveals a focused electric field. *Nature*. 427:548–553. http://dx.doi.org/10.1038/nature02270

Subbiah, R.N., C.E. Clarke, D.J. Smith, J. Zhao, T.J. Campbell, and J.I. Vandenberg. 2004. Molecular basis of slow activation of the human ether-a-go-go related gene potassium channel. *J. Physiol.* 558:417–431. http://dx.doi.org/10.1113/jphysiol.2004.062588

Subbiah, R.N., M. Kondo, T.J. Campbell, and J.I. Vandenberg. 2005. Tryptophan scanning mutagenesis of the HERG K+ channel: the S4 domain is loosely packed and likely to be lipid exposed. *J. Physiol.* 569:367–379. http://dx.doi.org/10.1113/jphysiol.2005.097386

Subbotina, J., V. Yarov-Yarovoy, J. Lees-Miller, S. Durdagi, J. Guo, H.J. Duff, and S.Y. Noskov. 2010. Structural refinement of the hERG1 pore and voltage-sensing domains with ROSETTA-membrane and molecular dynamics simulations. *Proteins*. 78:2922–2934. http://dx.doi.org/10.1002/prot.22815

Tan, P.S., M.D. Perry, C.A. Ng, J.I. Vandenberg, and A.P. Hill. 2012. Voltage-sensing domain mode shift is coupled to the activation gate by the N-terminal tail of hERG channels. *J. Gen. Physiol.* 140:293–306. http://dx.doi.org/10.1085/jgp.201110761

Tao, X., A. Lee, W. Limapichat, D.A. Dougherty, and R. MacKinnon. 2010. A gating charge transfer center in voltage sensors. *Science*. 328:67–73. http://dx.doi.org/10.1126/science.1185954

Tiwari-Woodruff, S.K., C.T. Schulteis, A.F. Mock, and D.M. Papazian. 1997. Electrostatic interactions between transmembrane segments mediate folding of Shaker $K^+$ channel subunits. *Biophys. J.* 72:1489–1500. http://dx.doi.org/10.1016/S0006-3495(97)78797-6

Trudeau, M.C., J.W. Warmke, B. Ganetzky, and G.A. Robertson. 1995. HERG, a human inward rectifier in the voltage-gated potassium channel family. *Science*. 269:92–95. http://dx.doi.org/10.1126/science.7604285

Viloria, C.G., F. Barros, T. Giráldez, D. Gómez-Varela, and P. de la Peña. 2000. Differential effects of amino-terminal distal and proximal domains in the regulation of human erg $K(^+)$ channel gating. *Biophys. J.* 79:231–246. http://dx.doi.org/10.1016/S0006-3495(00)76286-2

Wang, S., S. Liu, M.J. Morales, H.C. Strauss, and R.L. Rasmusson. 1997. A quantitative analysis of the activation and inactivation kinetics of HERG expressed in *Xenopus* oocytes. *J. Physiol.* 502:45–60. http://dx.doi.org/10.1111/j.1469-7793.1997.045bl.x

Wynia-Smith, S.L., A.L. Gillian-Daniel, K.A. Satyshur, and G.A. Robertson. 2008. hERG gating microdomains defined by S6 mutagenesis and molecular modeling. *J. Gen. Physiol.* 132:507–520. http://dx.doi.org/10.1085/jgp.200810083

Yifrach, O., and R. MacKinnon. 2002. Energetics of pore opening in a voltage-gated K(+) channel. *Cell*. 111:231–239. http://dx.doi.org/10.1016/S0092-8674(02)01013-9

Zagotta, W.N., T. Hoshi, and R.W. Aldrich. 1994. *Shaker* potassium channel gating. III: Evaluation of kinetic models for activation. *J. Gen. Physiol.* 103:321–362. http://dx.doi.org/10.1085/jgp.103.2.321

Zhang, M., J. Liu, and G.N. Tseng. 2004. Gating charges in the activation and inactivation processes of the HERG channel. *J. Gen. Physiol.* 124:703–718. http://dx.doi.org/10.1085/jgp.200409119

Zhang, M., J. Liu, M. Jiang, D.M. Wu, K. Sonawane, H.R. Guy, and G.N. Tseng. 2005. Interactions between charged residues in the transmembrane segments of the voltage-sensing domain in the hERG channel. *J. Membr. Biol.* 207:169–181. http://dx.doi.org/10.1007/s00232-005-0812-1